A Data-driven Approach to Multi-ring Basins Identification on Mercury

A. Sepe[1,2], L. Ferranti[2], V. Galluzzi[1], G. W. Schmidt[1], and P. Palumbo[1]

[1]INAF, Institute for Space Astrophysics and Planetology, Rome, Italy (antonio.sepe@inaf.it) | [2]University of Naples "*Federico II*", Department of Earth Sciences, Environment and Resources, Naples, Italy

EGU European Geosciences Union
Vienna 3–8 May 2026

SCAN ME

{ 1. Introduction & Dataset }

Multi-ring impact basins are among the oldest and most degraded large-scale impact structures on terrestrial planetary bodies [1]. On Mercury, several candidates were initially proposed based on Mariner 10 imagery, but not confirmed by subsequent MESSENGER-based analyses [2], highlighting the difficulty of recognizing ancient, heavily modified basin architectures.

Here we present a **semi-automatic, data-driven approach** for their systematic identification and characterization (Fig. 1).

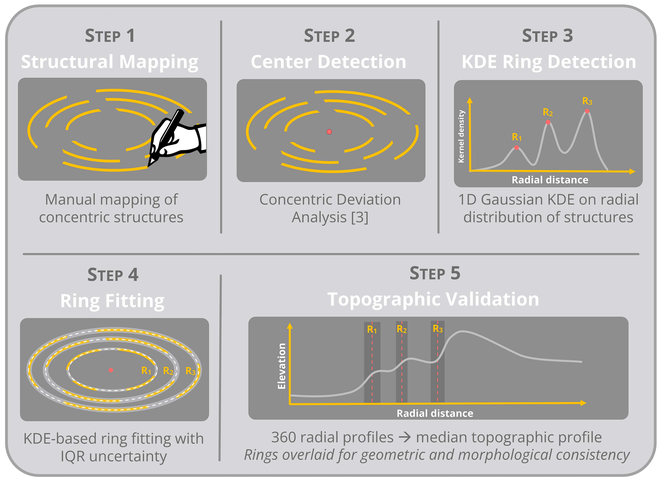

Figure 1. *Schematic diagram illustrating the semi-automatic workflow developed for the systematic identification and characterization of multi-ring impact basins.*

The workflow was first applied to the **Orientale basin** on the Moon (Fig. 2) as a validation test, given its well-constrained multi-ringed geometry [4], and subsequently extended to **eight candidate multi-ring basins on Mercury** (Tab. 1, Fig. 3).

Orientale analyses are based on the SLDEM2015 digital terrain model (DTM) [5] and the published ring map from [4]. For hermean basins, the USGS global DTM [6] and the v1.3 MerCatSS structural map [7] were used.

{ 2. Orientale Basin }

The workflow applied to the lunar Orientale basin identifies **three concentric rings** corresponding to the Inner Rook Ring (R ~ 250 km), Outer Rook Ring (R ~ 300 km), and Cordillera Ring (R ~ 450 km), consistent with previous studies [4]. The inferred ring geometry is further confirmed by the median radial topographic profile, which shows clear morphological expression at the predicted ring locations.

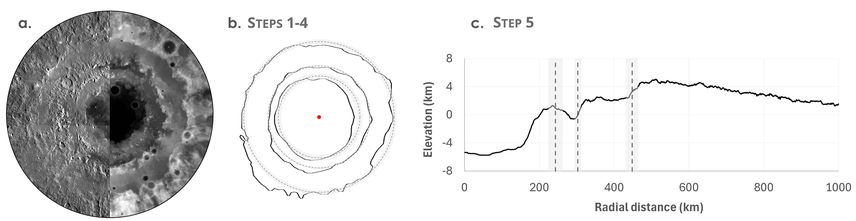

Figure 2. *Application of the workflow to the Orientale basin (Moon). a. (left) LROC WAC mosaic of the basin, (right) SLDEM2015 DTM [5]. b. Mapped concentric structures from [4] and KDE-inferred ring geometry (Steps 1–4). c. Median radial topographic profile (Step 5); dashed vertical lines indicate the three detected ring locations and their IQR uncertainty.*

{ 3. Hermean Basins }

The workflow was applied to **eight candidate multi-ring basins on Mercury** with different confidence levels, revealing multi-ringed geometries ranging from **3 to 6 concentric rings** (Tab. 1, Fig. 3).

All basins share a common general morphology (Fig. 4): a central **inner cavity (C)**, a **terrace** (or collapse annulus, **T**) connecting the cavity to the outer rim, and a **rim (R)**. The detected rings are predominantly located on the terrace, while most of the innermost and outermost rings correspond to the inner cavity border and the rim, respectively.

Table 1. *Number and extent of rings resulting from our workflow. The diameters marked in bold are considered as reference diameters in this study.*

Basin Name	# Rings	Diameter [km]
Sanai	4	220/272/392/**474**
Beethoven	5	284/338/440/522/**628**
Rembrandt	3	396/536/**706**
Sobkou	4	266/452/630/**804**
Calder-Hodgkins	5	202/716/1052/1244/**1464**
Andal-Coleridge	4	774/1134/1344/**1550**
Caloris	6	380/692/964/1146/1446/**1696**
Lennon-Picasso	6	652/1016/1200/1390/1600/**1822**

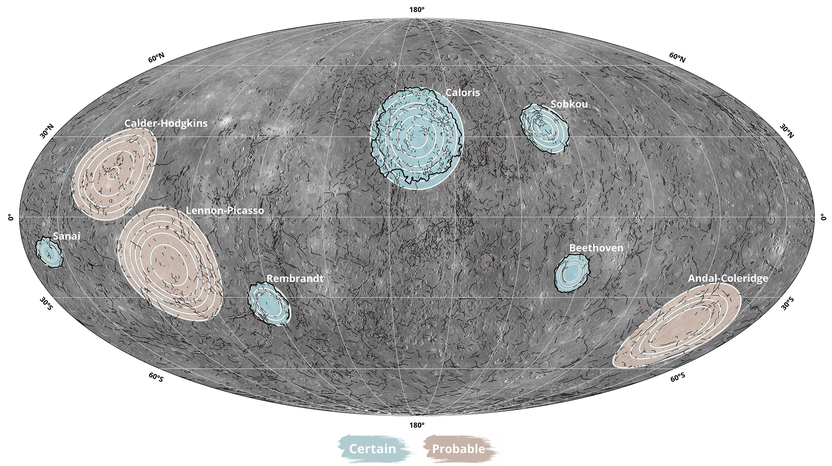

Figure 3. *The eight impact basins investigated in this study and their computed multi-ringed geometry. Thick black lines identify the rim of certain basins. MerCatSS global structural map overlaid to the global MDIS BDR basemap.*

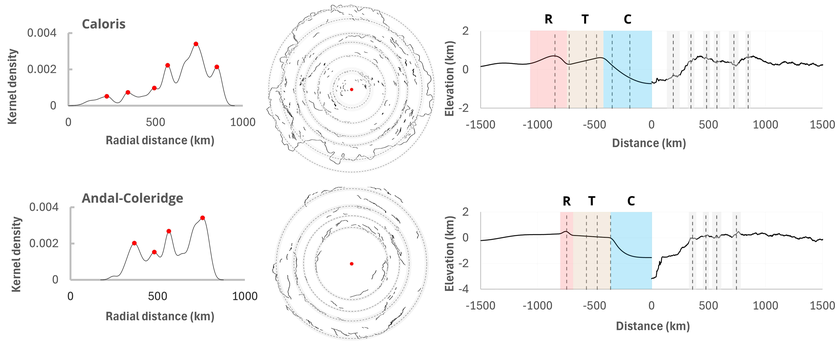

Figure 4. *Two representative examples illustrating the workflow performance on both well-preserved and heavily degraded basins architectures. (top) Caloris (certain, D ~ 1700 km) and (bottom) Andal-Coleridge (probable, D ~ 1550 km),*

{ 4. Ring spacing & Morphology}

Ring diameters (Tab. 1) were compared across all eight basins to assess the consistency of the $\sqrt{2}D$ **spacing law** previously proposed for the Moon, Mars, and Mercury itself [8]. When plotted on a log-log diagram (Fig. 5), the detected rings (D_R) align along discrete lines corresponding to fixed fractions of the basin diameter (D_B), revealing two distinct sequences. The **main sequence** follows the theoretical $\sqrt{2}D$ spacing, consistent with previous observations [8].

A **secondary sequence** is identified here, falling systematically between the main sequence lines and present across basins of different sizes and confidence levels.

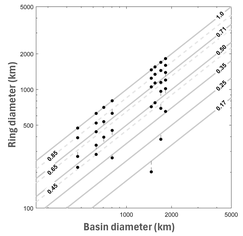

Figure 5. *Ring diameter vs. basin diameter for all detected rings. Solid lines represent the theoretical $\sqrt{2}D$ spacing (D_R/D_B = 1, 0.71, 0.5, 0.35, 0.25, 0.17). Dashed lines identify a secondary sequence at ~0.2D spacing (D_R/D_B = 0.45, 0.65, 0.85).*

The morphological scaling of key basin features was investigated by comparing the inner cavity radius (*r*), terrace width (W_T), and the cavity-to-rim ratio (*r/R*) with the rim radius (*R*). The inner cavity radius (Fig. 6a) scales linearly with the basin size, yielding an approximately constant ratio of **r/R ~ 0.5** across the sample. The terrace width follows a similar scaling (Fig. 6b). Plotting the r/R ratio against rim radius (Fig. 6c), **multi-ring basins** show a scattered distribution for R < 400 km before converging to r/R ~ 0.5 for larger basins, similarly to **peak-ring basins**.

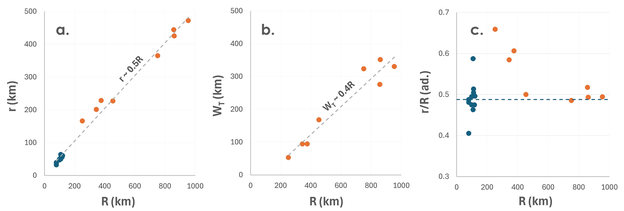

Figure 6. *Morphological scaling of hermean multi-ring (orange) and peak-ring basins (blue). a. Inner cavity radius (r) vs. rim radius (R). b. Terrace width (W_T) vs. rim radius (R). c. Cavity-to-rim radius ratio (r/R) vs. rim radius (R) where the dashed blue line represent the average r/R value for peak-ring basins.*

{ 5. Conclusions & Future Works}

With our workflow we have recognised **eight potential multi-ring basins on Mercury**, surrounded by a system of **3-to-6 concentric rings**. Ring spacing appears to follow the $\sqrt{2}D$ **spacing law**, consistent with previous observations. A **secondary ring sequence** at ~0.2D is identified.

The eight basins share a common general morphology with a central cavity, a terrace and a rim. Together, the central cavity and the terrace account for **~90% of the total basin radius** (~50% and ~40% respectively).

Multi-ring basins show a scattered distribution of r/R values for R < 400 km, before converging to typical peak-ring values of **r/R ~ 0.5** for larger basins. This convergence suggests a common morphological attractor shared by both basin classes, while the scatter at smaller sizes may reflect differential post-impact modification or a transitional morphological regime.

Future work will extend this workflow to additional hermean basins and investigate the origin of the secondary ring sequence and the r/R transition at R ~ 400 km.

{ References } [1] Spudis (1993). In: *The Geology of Multi-Ring Impact Basins: The Moon and Other Planets*, XI-XII. [2] Fassett et al. (2012). *JGR: Planets*, 117.E12. [3] Karagoz et al. (2024). *JGR: Planets*, 129(1). [4] Whitten et al. (2011). *JGR: Planets*, 116.E6. [5] Barker et al. (2015). *Icarus*, 273, 346-355. [6] Becker et al. (2016). *47th LPSC*, Abstract #1903. [7] Bernhardt et al. (2025). *EPSC-DPS 2025*, Abstract #2108. [8] Pike & Spudis (1987). *Earth, Moon, and Planets*, 39(2), 129-194.

~ We gratefully acknowledge funding from the Italian Space Agency (ASI) under ASI–INAF agreement 2024–18–HH.0 ~